Int J Earth Sci (Geol Rundsch)
DOI 10.1007/s00531-007-0169-z

ORIGINAL PAPER

Erosion rates on subalpine paleosurfaces in the western Mediterranean by in-situ ^{10}Be concentrations in granites: implications for surface processes and long-term landscape evolution in Corsica (France)

Joachim Kuhlemann · Klaas van der Borg · Paul D. Bons · Martin Danišík · Wolfgang Frisch

Received: 1 December 2005 / Accepted: 1 November 2006

Abstract A study of erosion rates by in-situ ^{10}Be concentrations in granites of Miocene high-elevation paleosurfaces in Corsica indicates maximum erosion rates between 8 and 24 mm/kyear. The regional distribution of measured erosion rates indicates that the local climatic conditions, namely precipitation, the petrographic composition of granites, and the degree of brittle deformation govern erosion rates. Chemical erosion dominates even at elevations around 2,000 m in presently subalpine climate conditions. Field evidence indicates that erosion operates by continuous dissolution and/or disintegration to grains (grusification). The erosion rates are relatively high with respect to the preservation of inferred Early Miocene landscapes. We infer temporal burial in the Middle Miocene and significantly lower erosion rates in the Neogene until ~3 Ma to explain the preservation of paleosurfaces, in line with fission track data. Valley incision rates that are a magnitude higher than erosion rates on summit surfaces result in relief enhancement and long-term isostatic surface uplift. On the other hand, widening and deepening of valleys by cyclic glaciation progressively destroys the summit surface relics.

Keywords Erosion rates · Cosmogenic · Beryllium · Subalpine climate · Paleorelief · Granite

J. Kuhlemann (✉) · P. D. Bons · M. Danišík · W. Frisch
University of Tübingen, Institute of Geosciences, Sigwartstrasse 10, 72076 Tübingen, Germany
e-mail: kuhlemann@uni-tuebingen.de

P. D. Bons
e-mail: paul.bons@uni-tuebingen.de

M. Danišík
e-mail: martin.danisik@uni-tuebingen.de

W. Frisch
e-mail: wolfgang.frisch@uni-tuebingen.de

K. van der Borg
Subatomic Physics Department, Van de Graaff Laboratory, Utrecht University, P.O. Box 80.000, 3508 TA Utrecht, The Netherlands
e-mail: K.vanderborg@phys.uu.nl

Introduction

Extremely low erosion rates in the range of 0.1 mm/kyear are known from arid to hyperarid environments on Earth, where landscapes are preserved for tens of million years (e.g. Brook et al. 1995; Bierman and Turner 1995; Cockburn et al. 2000). Fairly low erosion rates in the range of 2–15 mm/kyear are reported from alpine environments on high-elevation summit surfaces in western America (Small et al. 1997). These summit surfaces may represent relics of ancient landscapes. They appear to be stable geomorphic features, since ongoing physical weathering and regolith creep conserve their shape (Small and Anderson 1998; Anderson 2002). The assumption of geomorphic stability, however, may conflict with the globally observed relief enhancement, possibly caused by increased climate variability since the late Pliocene (Zhang et al. 2001). It is not quite clear to what degree erosion rates in granite are controlled by climate or by relief (Riebe et al. 2000).

The North American summit surfaces probably formed before mid-Cenozoic times, since the paleorelief of the apparently younger sub-summit surface on the eastern flank of the Rocky Mountain Front Range

became locally sealed by volcanic rocks associated with the Rio Grande rift (Seager et al. 1997). The question arises if preservation of ancient high-elevation landscapes for several million years, despite differential uplift and climate change, may be a common feature. In this paper, we present cosmogenic nuclide data from relics of subalpine to alpine paleosurfaces of Corsica (western Mediterranean), which have much in common with their western North American counterparts. The aim of this study is to show how climatic and lithologic factors influence weathering style and erosion rates in granite landscapes, and what this implies for long-term landscape evolution.

Regional setting

The island of Corsica is situated in the northwestern Mediterranean basin, between 41° and 43° latitude, covering an area of 8,722 km^2 (Fig. 1). Corsica is formed by a Late Paleozoic Variscan basement in the west, and a smaller Alpine orogenic wedge in the east, which represents the southern continuation of the Western Alps. The western margin of Corsica experienced Oligocene rifting (Ferrandini et al. 1999) and subsequent eastward drifting away from the European margin (Vigliotti and Langenheim 1995). Apatite fission track data (Zarki-Jakni et al. 2004; Danisik 2005) show that fast cooling between 30 and 25 Ma as a consequence of rifting was followed by slow cooling of Variscan Corsica since the Early Miocene. Modelling of apatite fission track length measurements (Fig. 2) indicates stagnation of cooling from about 25 Ma until late Neogene times in central Variscan Corsica, suggesting very low erosion rates (Kuhlemann et al. 2005a). Major sinistral faulting and tilting occurred during Early Miocene differential counter-clockwise rotation (Gorini et al. 1993). The Alpine wedge on the eastern side of Corsica experienced Late Oligocene to

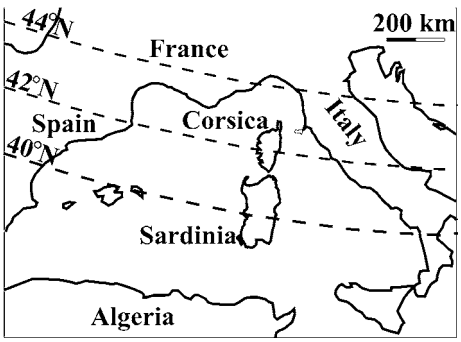

Fig. 1 Geographic location of Corsica

Middle Miocene extension (Brunet et al. 2000; Cavazza et al. 2001), which turned to uplift in the Late Miocene (Orszag-Sperber and Pilot 1976; Ferrandini et al. 1998).

The Variscan basement block is largely composed of Carboniferous calc-alkaline granites (Rossi and Cocherie 1991). Some Permian rhyolite and alkaline granite massifs rise above surrounding calc-alkaline granites (Fig. 3b). Gneisses are subordinate. Eocene greywacke and meta-greywacke partly cover the eastern margin of Variscan Corsica. Intrusive rocks are largely undeformed, except for widely spaced SW-NE striking faults, and brittle deformation along the eastern margin of Variscan Corsica (Seidl 1978).

Variscan Corsica displays a moderate-to-rugged relief up to 2,706 m in height (Fig. 3a), with average slopes of 25° in calc-alkaline granites and 30° in alkaline granites and rhyolites (Kuhlemann et al. 2005a). Two levels of paleosurfaces exist, preserved as isolated relics up to 30 km^2 in size. The summit surface fragments (Fig. 3c) are locally tilted by up to 20° and some faults responsible for tilting are sealed by a mid-elevated ''piedmont'' paleosurface in southern Corsica. Several lines of evidence, including facies, deformation, and tilt of local Miocene basins, suggest an Early Miocene formation age for the summit surface (Kuhlemann et al. 2005a). Both paleosurface generations have been upwarped in the east after 10 Ma, contemporaneously with uplift of the Alpine wedge in Eastern Corsica (see Orszag-Sperber and Pilot 1976). Late Pleistocene uplift, indicated by marine notches and terraces of the last interglacial, yields rates up to 300 mm/kyear in the NW, but generally about 50 mm/kyear in the SW (Kuhlemann et al. 2005a). Local recent uplift in the W is confirmed by precise levelling measurements (Lenôtre et al. 1996). Knickpoints in longitudinal river profiles, related to Miocene paleosurfaces, however indicate that fluvial incision has not yet equilibrated with relief.

The recent climate of Corsica at sea level is characterized by subtropical Mediterranean-type conditions with a dry and warm summer and a temperate wet winter. Average annual precipitation increases from ca. 600 mm/year on the coast to more than 1,500 mm/year inland (Bruno et al. 2001; Fig. 3d). Advection of moisture both from westerly and southeasterly directions causes a roughly symmetric distribution of precipitation, except for the drier interior in the northern center. Episodic torrential precipitation events, as testified by meteorologic observation (Bruno et al. 2001) and bedload size in rivers, occur particularly along the southeastern margin of the mountains. The highest sampling sites located in subalpine envi-

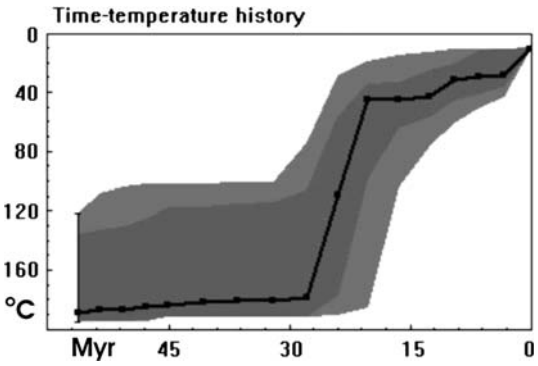

Fig. 2 Cooling path of Monte Carlo-modelled apatite fission track length measurements of a sample taken from the summit surface of southern Corsica (location IV in Fig. 3). The *inner dark grey envelope* shows the best fit time-temperature path with a merit function value of 0.05, the *light grey envelope* a merit function value of 0.5 (AFTSolve®, Ketcham et al. 2000). These modelled thermal data cannot be directly translated to erosion rates, since temporal variations of the thermal gradient remain unknown and surface cooling related to climate change and surface uplift is not included

ronment at elevations of 2,300 m are characterized by frost for half of the year. Along the drainage divide and at the extremities of the island, wind speed frequently exceeds 20 m/s and may even exceed 50 m/s (Bruno et al. 2001).

During stadials of the late Pleistocene, average temperatures in alpine environments were lowered by about 8°C, according to reconstruction of the equilibrium line altitude of ancient glaciers (Kuhlemann et al. 2005b). This estimate matches sea surface temperature lowering in the western Mediterranean basin (Cacho et al. 2002; Hayes et al. 2005). Thus, the mountains of Corsica above about 1,500 m were glaciated (see Conchon 1986). Preservation of the summit surface is poor in northern and central Corsica, due to modification by valley glaciers (Kuhlemann et al. 2005b). In contrast, the southernmost summit surface in the Cagna massif, which at elevations between 1,000 and 1,300 m remained unglaciated, represents the best-preserved ancient landscape. Here, a cut-off meander as part of an Early Miocene river is preserved (Kuhlemann et al. 2005a).

Methods

Sampling sites for ^{10}Be on the flat summit surfaces were chosen to be above the level of Pleistocene glaciers, and to be exposed to wind and solar radiation to minimize shielding by snow and ice during stadials. Effects of topographic shielding, ranging between 2° and 8°, are low. Samples were taken from planar tops

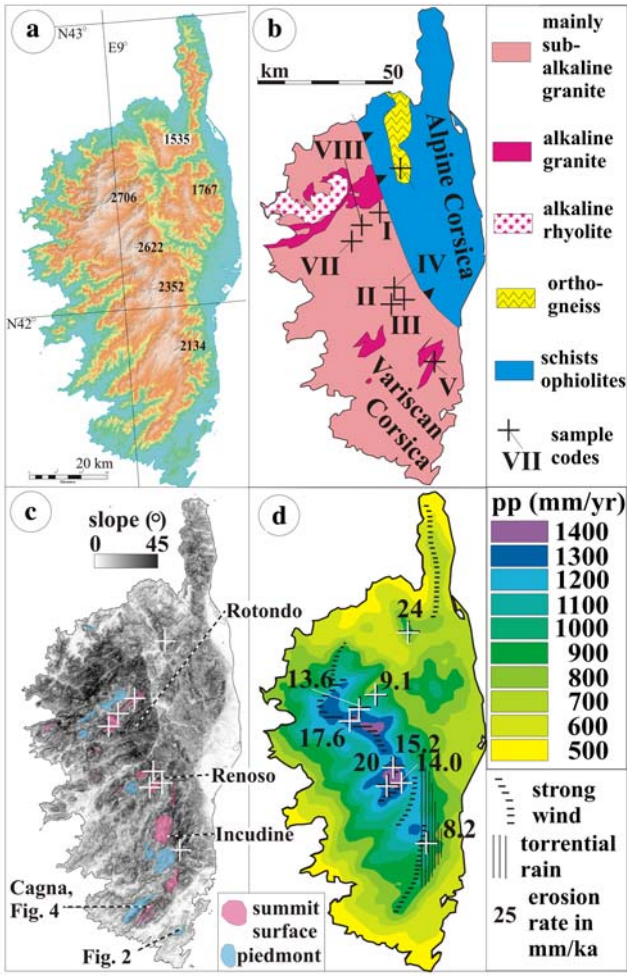

Fig. 3 **a** Digital Elevation Model of Corsica. *Numbers* indicate peak elevation in meters. **b** Simplified sketch map of lithologies in Corsica with sampling locations. **c** Map of the slope distribution calculated from the Digital Elevation Model. *Light colors* at high elevation (see **a**) indicate paleosurfaces. Small remnants of the summit surface are indicated by *arrows*. **d** Distribution of annual precipitation (pp) in Corsica according to Bruno et al. (2001), and zones of torrential rain and strong wind

of bedrock knobs (tors) rising at least several meters above the summit surface. At site VIII, the summit surface is almost totally destroyed, and the peak of the mountain is equivalent to the top of a tor, surrounded by a blanket of boulders. At the sampling sites I and II, a core of 40 mm diameter was drilled down to 30 cm depth on the top of tors for consistency tests. The surface samples represent the topmost 2 cm of bedrock at the site. Elevation and latitude were determined from French IGN 1:25,000 topographic maps.

Chemical treatment generally followed Kohl and Nishiizumi (1992). After optical evaluation and XRF control measurements of Al and trace element contents, purified quartz samples of 15 to 50 g were pre-

pared for accelerator mass spectrometry (AMS) measurements at Utrecht.

^{10}Be forms when oxygen nuclei within quartz are exposed to high-energy cosmic ray particles (Nishiizumi et al. 1989). The production of ^{10}Be (P) decreases with depth (z) according to the equation:

$$P(Z) = P_0 e^{-z/z*},$$

where the scale length $z^* = \Lambda/\rho$, is the ratio of the absorption mean free path (Λ) of 157 g/cm^2 (Lal 1991) and the density of the solid (ρ), here granite and gneiss of 2.7 g/cm^3.

For local surface production rates (P_0) and latitude-elevation coefficients we applied the now commonly used calculation of Dunai (2000, 2001a), instead of Lal (1991). We assumed an average air pressure of 1,014 hPa at sea level for the last 20–60 ka instead of the recent range between 1,015 and 1,016 hPa, due to higher cyclon frequency (Kuhlemann et al. 2005b). For average sea-level temperature, we used the marine paleo-temperature record of Cacho et al. (2002) and the nominal exposure age to recalculate the time-integral of temperature. The potential error of these two effects in the calculation of ^{10}Be-production is about 2%. We estimate the potential systematic error resulting from snow shielding as to be about 2%, since all sampling sites are exposed to wind and insolation. For sea-level high-latitude ^{10}Be-production rates, we had to decide between a lower value of 5.1 atoms/g/year by Stone (2000), a higher value of 5.53 atoms/g/year of Schaller et al. (2002, with references) which includes 0.199 atoms/g/year muon contribution, and an intermediate value of 5.44 atoms/g/year including muon contribution by Kubik and Ivy-Ochs (2004), which is a recalculation of Kubik et al. (1998). We prefer the last production rate because it is based on a central European calibration site, which is relatively close to our study area. The potential error of the production rate is estimated at 5%. We considered the effect of secular variations of the earth's magnetic field for nuclide production calculated by Dunai (2001b), but corrections are below 1%. We calculate the total 1σ error of our data as the sum of independent errors. Applying another production rate only results in a minor shift of the absolute values obtained, without a relevant change of relative differences between the sites.

For a calculation of maximum erosion rates (ε) in surface samples we assume a dynamic equilibrium of erosion rates and nuclide production rates on the timescale of 100 ka (see Clark et al. 1995), which ideally represents steady-state:

$$N_{(0)} = \frac{P_0}{\left(\frac{\varepsilon}{Z^*}\right) + \lambda} \Rightarrow \varepsilon = Z * \left(\frac{P_0}{N_{(0)}} - \lambda\right)$$

The decay constant λ of ^{10}Be is 1.51 Ma^{-1} (Gosse and Phillips 2001). According to Small et al. (1997) the assumption of steady-state erosion is hardly valid in alpine settings. However, we will present field evidence, which makes the assumption of steady-state erosion reasonable.

Field evidence

Field evidence plays an essential role in this study as to constrain which weathering processes shape geomorphic features of various scale.

The summit surface relics in southern Corsica (Cagna and Incudine Massivs; Figs. 3c, 4, 5) display largely vegetated flats with isolated tors, steep hills built of calc-alkaline granite boulders, and up to 200 m high rock castles with a boulder mantle. The size of boulders decreases with increasing distance from the rock castle. Regional variation of the boulder size depends on the spacing of joints. The rock castles are surrounded by rarely exposed grusy bedrock with a 0.5 m to few meter-thick regolith cover of granite grains with some elongated granite blocks of few dm-size and angular dyke pieces. The blocks are concentrating on

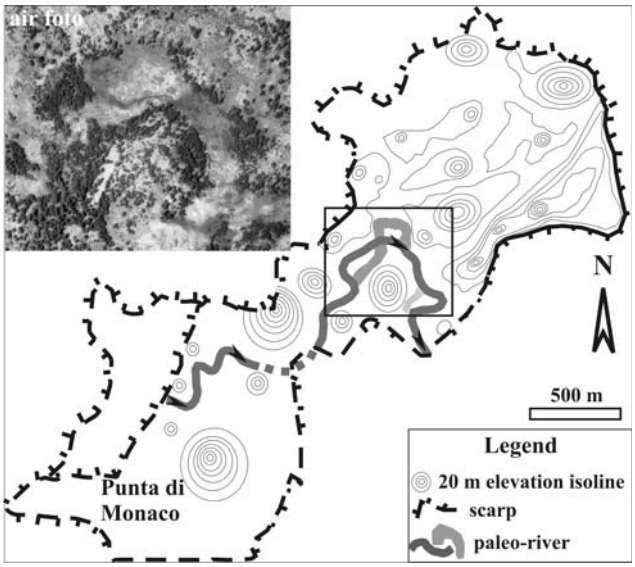

Fig. 4 Sketch map of the summit surface relict in the Montagne de Cagna in the southern end of Corsica (see Fig. 3c) with reconstructed course of the paleoriver. The direction of flow is speculative (modified from Kuhlemann et al. 2005a, b). The *air photo* shows a blow-up of the meander in the black frame

Fig. 5 Typical summit surface in southern Corsica on the largest preserved plateau in the Incudine Massif (see Fig. 3c), situated in the upper montane zone where forest was cleared. The rock castle in the background (1,745 m) rises 200 m above the valley floor

top of the regolith, since they are weathering slower than the smaller regolith components. In central and northern Corsica, rock castles are smaller and rise up to 30 m, surrounded by regolith which locally forms a periglacial flat (Fig. 6a–f).

Such high periglacial flats are only locally found above Pleistocene valley glaciers on the summit surface fragments. The Wurmian maximum glacier extent is constrained by trimlines (Kuhlemann et al. 2005b; Fig. 7). The Pleistocene glaciers of Corsica were formed of wet-based temperate ice, typical for a maritime climate. The erosiveness of the ice is testified by the common occurrence of roche moutonnée in most valleys. Below the snowline, trimlines are present in steep U-shaped valleys whereas till limits and kame terraces are preserved on moderate slopes.

Although periglacial climate conditions in general favour spallation of blocks (see Small et al. 1997), platy block fragments are subordinate on top of the regolith of summit surfaces below 2,200 m a.s.l. Above 2,200 m, the number of platy block fragments gradually increases depending of the granite type as climate conditions change from subalpine to alpine. However, even the highest sampling site IV at 2,352 m is dominated by grusification.

Apart from grusification, Tafoni-type concave weathering contributes to regolith formation. In recent active sites below c. 1,700 m a.s.l., Tafoni weathering produces millimeter-sized granite chips crosscutting mineral boundaries, or millimeter-thick small grusy granite plates. Some rock castles located between c. 2,000 and 1,800 m a.s.l. have been affected by Tafoni-type weathering, which is currently inactive as testified by moss and lichen cover. The rate of Tafoni formation at such altitudes is deduced from geomorphic evidence. Narrow active Tafoni cavities of 50 cm depth (Fig. 8), formed in situ in a moraine boulder deposited in the late Wurmian at 1,500 m a.s.l. north of Col de Vergio (Conchon 1985; photo 1, Fig. 1), indicate that the Holocene was too short to allow for the formation of meter-sized Tafoni found around 1,800 m a.s.l. Consequently, meter-sized Tafoni at 1,800–2,000 m a.s.l. must have been formed prior to the last glaciation, during warm interglacial periods (see Klaer 1956). As grusification and dissolution continued to erode the top side of fossil Tafoni blocks at 1,800 m a.s.l., the dm-thin Tafoni roofs of the cavity were penetrated and finally Tafoni blocks broke apart. Large Tafoni skeletons lie in rather unstable position on bare granite bedrock of the summit surface, about 100 m above the local Wurmian snowline minimum (Kuhlemann et al. 2005b; Fig. 12). It is, however, unlikely that such fragile objects could withstand the pulling force of temperate ice. Accumulation of snow and ice in this site seems to have been surpressed by wind and insolation as typical for flat ridges in Corsica (Fig. 9).

Wind plays a role for erosion along the main drainage divide, as testified by desert pavements on periglacial flats. An isolated boulder, resting on a narrow base of grusy granite on the edge of the summit surface in the Renoso massiv, is streamlined by dominant westerly winds. This boulder is densely covered by lichens on the top and the windward face, indicating that the lichens protect the rock rather than accelerating erosion by etching (Fig. 10). In regions without strong wind, boulders surrounding rock castles have a similar top cover of lichens, but show micro-scale etching on the rain-protected, lichen-free bottom sides. The etching produced a smooth, deep, concave feldspar matrix (plagioclase and alkali feldspar) in which slightly etched sharp-edged quartz grains rise several millimeters above the surface. Probably the etching results from condensation of fog and clouds.

Evidence of etching of bare bedrock is found in various granite types at different slope angles, but especially in alkali-feldspar granites, where features such as karren, typical of massive limestone, have been described as ''pseudo-karst'' and ''silica karstification'' by Klaer (1956). On flat summit surfaces, networks of dm- to m-wide, dm-deep potholes and channels are typical (Fig. 11). Such networks are often governed by fissure systems. Nevertheless, few to several centimeter-deep initial pothole formation without visible working points at fissure junctions is observed on plucked off plane faces of moraine boulders, deposited in late glacial time (Conchon 1985, see above).

At elevations of 2,000–2,300 m in central Corsica (Rotondo massiv, up to 2,622 m a.s.l.), glacially-abra-

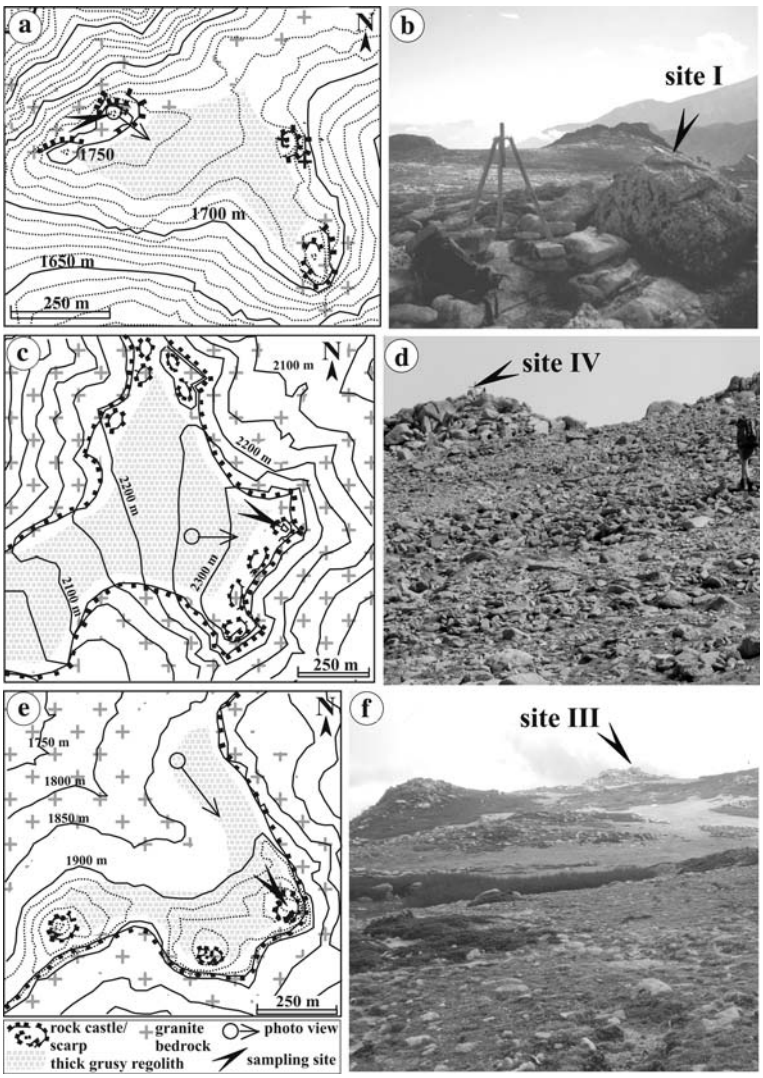

Fig. 6 Sketch maps and landscape of the sampling sites I (**a**, **b**), IV (**c**, **d**), and III (**e**, **f**). The summit surface at sites IV and III is surrounded by scarps, caused by plucking of glaciers. Note that the horizontal view suggests a high amount of blocks, whereas a vertical view would show that in reality only 20–40% of the surface is covered by blocks. Half of the blocks in photo (**d**) are andesitic dyke fragments

ded granites frequently show fine-grained durable relics of mafic enclaves with relics of glacial striations on limonitic crusts, indicating near zero erosion after final glacier retreat (Fig. 12). Exposure dating of this particular site yielded an age of 3.4 ± 0.6 ka (Table 1), without correction for 35 mm erosion and shielding by annual average snow cover, which we calculated at 0.8 m (40 g/cm^2) for the 2002–2006 record of a meteorologic station 700 m away (Meteo France [1]; see also Bruno et al. 2001, p. 61). Considering global warming of the last decades, an estimate of 50 g/cm^2 for the late Holocene seems realistic. Including these corrections, the exposure age would be 5.1 ± 1.3 ka. With respect to the Holocene record of global cooling (O'Brien et al. 1995) and glacier advances in the Alps (Hormes et al. 2001), we consider this age to reflect glacier abrasion at around 5.3 ka, assuming glacier retreat as late as 5.0 ka. Thus, the roche moutonnée in this particular site was subjected to calc-alkaline granite weathering and erosion of ~7 mm/kyear.

Petrography and texture of samples

Most samples represent coarse-grained (5–10 mm) monzogranite of central Corsica, composed of plagioclase, slightly perthitic microcline with quartz inclusions, polycrystalline quartz, and iron-rich biotite (Fig. 13). Hornblende is very rare. Biotite rims display iron mineral crusts from weathering. Samples VII and VIII are similar to sample I (Pinerole). In sample II, the biotite of the monzogranite is largely transformed into chlorite. Zoisite is present in fissures. The plagioclase is saussuritised. The texture of sample II shows common brittle deformation of quartz and feldspar

[1] http://www.meteofrance.com/FR/montagne/obs.jsp?LIEUID = MONT_MANIC

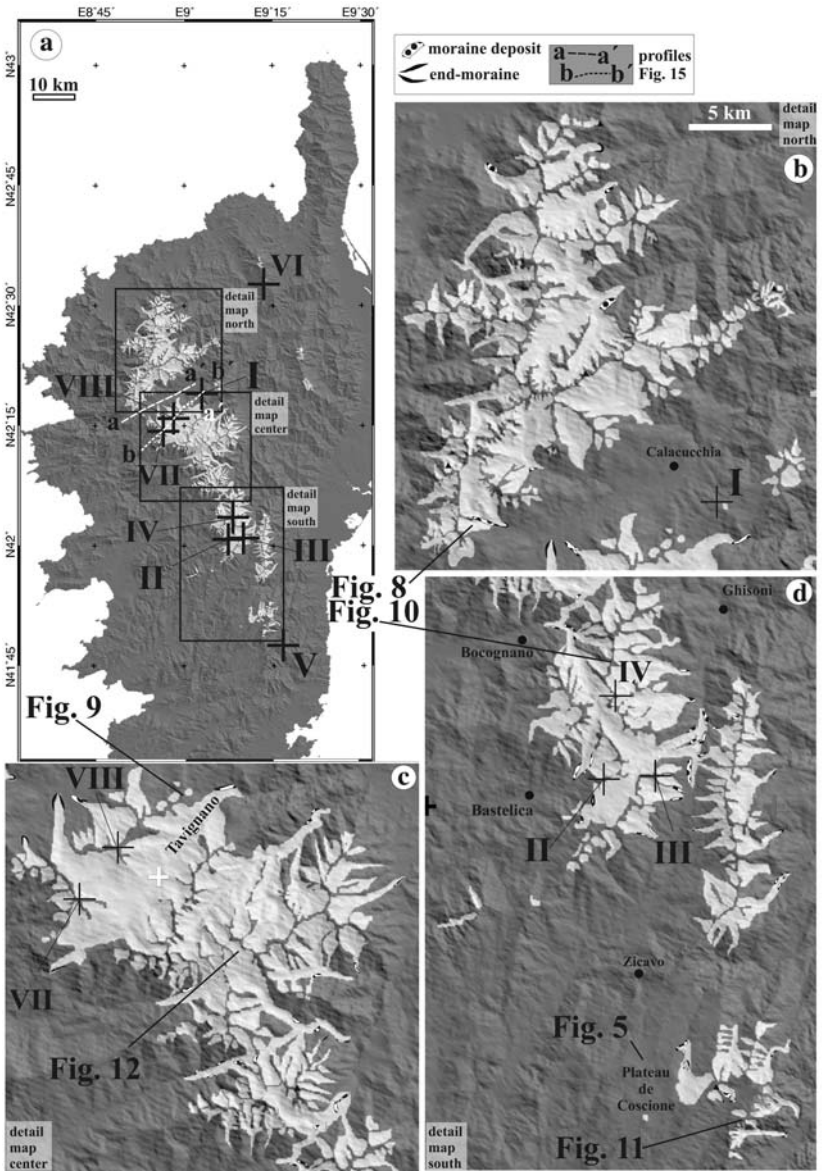

Fig. 7 Map of the Wurmian maximum glacier extension in Corsica, probably during MIS 4 (modified from Kuhlemann et al. 2005b)

(Fig. 13). Deformation lamellae in quartz grains are frequent. Samples III and IV from the same region display much less transformation of biotite, and less penetrative brittle deformation, which indicates localized brittle deformation and alteration.

Sample V is an acidic iron-rich alkali-feldspar granite composed mainly of perthite, quartz (~20%), and some hastingsite (Rossi et al. 1980). The rock does not contain plagioclase or biotite, but traces of fayalite and accessory magnetite, pyrrotite, zircon and fluorite are present. The grain size is fairly homogeneous and ranges between 3 and 8 mm. The durable rock lacks deformation features in hand specimen and thin section.

Sample VI is a plagioclase-rich, strongly foliated orthogneiss with quartz ribbons, sericite and chlorite as products of Alpine retrogression of former biotite. Brittlely deformed feldspar grains typically appear as sigma clasts, testifying top-to-the-east sense of shear that is related to Late Oligocene to Early Miocene extension (see Brunet et al. 2000). Brittle deformation of relatively small, recrystallized quartz grains is also common.

In-situ ^{10}Be erosion rates

We observe ^{10}Be concentrations between 0.37 and 1.25×10^6 atoms/g (Table 1). We interpret these data in terms of maximum erosion rates, assuming dynamic equilibrium of cosmogenic nuclide production and erosion (plus decay). This assumption is based on field

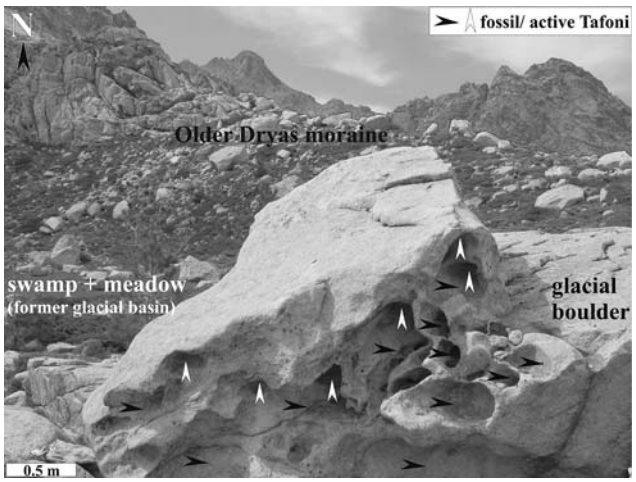

Fig. 8 Glacial boulder of the late Wurmian (Older Dryas) with concave Tafoni weathering that partly formed prior to glacial transport (fossil Tafoni, *black arrows*) and partly in situ (active Tafoni, *white arrows*; location in Fig. 7b). Tafoni weathering always migrates upwards

Fig. 10 Isolated boulder on the edge of the northernmost Renoso summit surface. The main wind direction is from left to right (W to E). Below the boulder, grusy weathering and disintegration into thin plates is visible (location in Fig. 7c). Note the crack at the base of the streamlined boulder (*arrow*) which shows that dominance of grusification does not exclude spallation of dm-sized chips

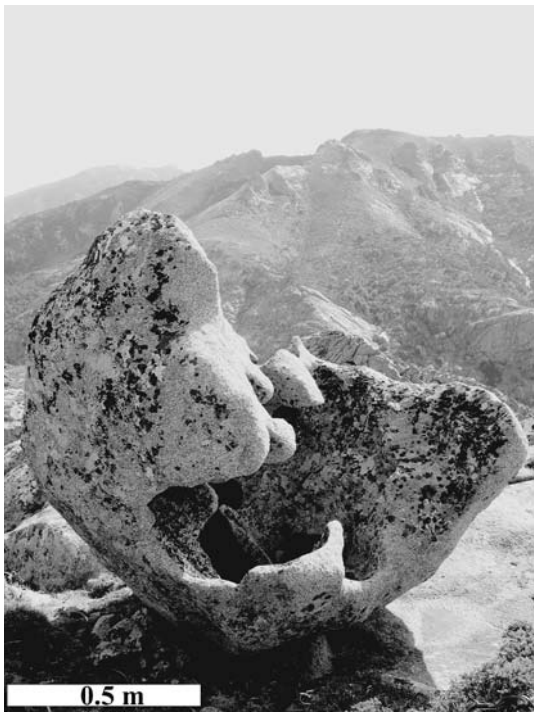

Fig. 9 Tafoni skeleton (1.5 m high) found at 1,788 m a.s.l. between sites I and VIII, which formed at this place, broke apart and left behind one piece that lies upside down on a slightly convex flat grusy ridge , while other smaller pieces fell down the ridge (location in Fig. 7d)

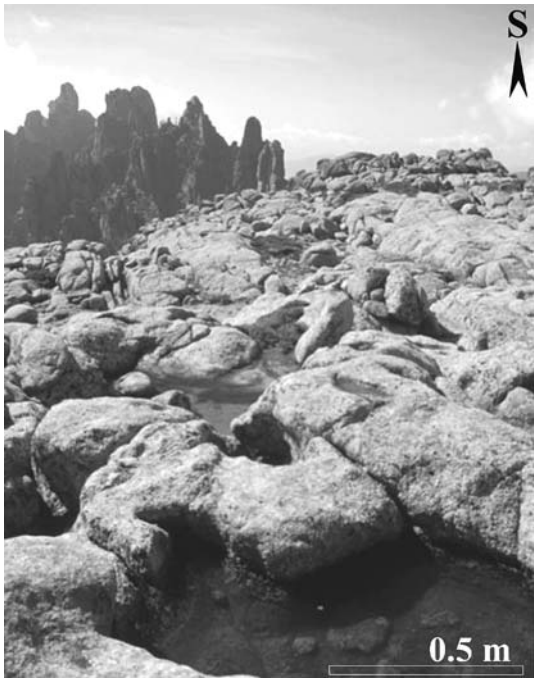

Fig. 11 View of the summit surface 5 km SE of the Incudine summit surface at c. 1,800 m, showing potholes as typical features of silica karstification in alkaline granite (location in Fig. 7d)

evidence listed above, which show that episodic spallation of larger rock pieces from tors on the summit surface is rare whereas fairly regular erosive processes such as dissolution and grusification is dominant. For comparison, we calculated exposure ages assuming zero erosion (Table 1).

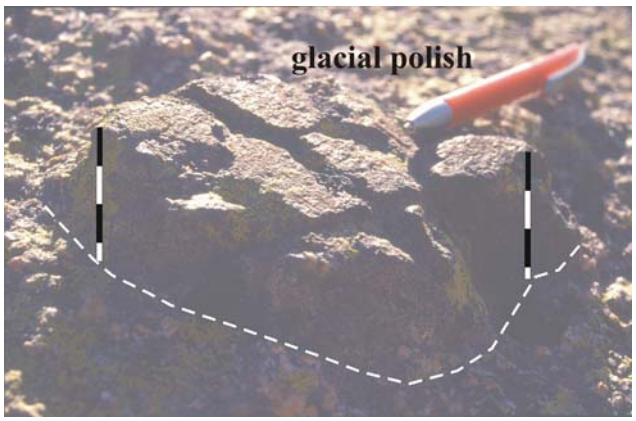

Fig. 12 Detail of a glacially polished fine-grained mafic enclave, rising 30–35 mm above coarse its calc-alcaline granite matrix. The scale bar is in cm, but also note the pen in the back for scale. The *arrow* indicates the direction of glacial striae. The site is located at 2,330 m a.s.l. in the island center on the south face the Rotondo massif (2,622 m in Fig. 3a; location in Fig. 7c)

Maximum erosion rates of the summit surface samples range between 8.2 and 24 mm/kyear (Table 1).

The erosion rates calculated for the surface samples show a combined climatologic and lithologic effect (Table 2; Fig. 3d). The lowest rate of 8.2 mm/kyear is found in alkali-feldspar granite, despite frequent torrential rain at this site (V). A low erosion rate of 9.1 mm/kyear is found in a calc-alkaline monzogranite in a zone of reduced precipitation (I). Medium erosion rates ranging from 13.6 to 17.6 mm/kyear are found on, or close to the main drainage divide in windy and rainy sites of weakly to moderately sheared calc-alkaline granite (III, IV, VII, VIII). Highest rates of 20 and 24 mm/kyear are found in calc-alkaline granite with intense shearing (II) and sheared orthogneiss (VI), respectively. Site II is more rainy than site VI, but erodibility apparently overcompensates the deficit in precipitation.

For the purpose of consistency tests, two cores (sites I, II) were sampled down to increasing depth (location in Fig. 3b). The fit of data with the modelled decrease of ^{10}Be concentrations with depth underpins the assumption that samples from the topmost 3 cm of bare rock are representative of maximum erosion rates within the range of error (Fig. 14, Table 2). However, in core I the topmost three samples yield very similar ^{10}Be concentrations which disturb the expected concentration profile, but fit within the range of error (Fig. 14). We speculate that in the topmost centimetres of the rock column a portion of the energy of cosmic ray particles is being lost by back-scattering (Masarik and Reedy 1996). This depth profile of ^{10}Be thus sug-

Table 1 Concentration of ^{10}Be in surface samples

Column 1	2	3	4			5			6	7	8	9	10	11	12	13	14
Sampling site	Code	Altitude (m)	N. latitiude			E. longitude			α Shield. Degrees	N: conc. ^{10}Be × 10^6 at/g	Error × 10^6 at/g	Analyt. error (%)	Corr. cos. prod. P^0(42) [at/(g year)	Erosion rate (mm/kyear)	1σ Error (mm/kyear)	Nom. expo. age (year)	1σ Error age (year)
			°	′	″	°	′	″									
Pinerole/Niolu	I	1,759	42	18	47	09	02	55	4	1.23	0.11	8.94	19.79	9.1	1.0	63,219	7,311
Plateau d'Ese	II	1,759	42	00	00	09	07	06	5	0.55	0.11	20	19.54	20.3	4.3	28,441	6,058
Mte Giovanni	III	1,950	41	00	00	09	09	14	3	0.92	0.12	13	22.59	14.0	2.1	41,171	6,160
Mte Renoso	IV	2,352	42	03	36	09	08	04	2	1.14	0.12	10.5	30.32	15.2	2.0	37,953	4,870
Bavella	V	1,420	41	46	36	09	14	15	8	1.03	0.25	24.3	15.13	8.2	2.1	69,861	17,699
Tenda	VI	1,453	42	30	58	09	15	02	5	0.37	0.09	24.3	15.64	24.2	6.2	23,879	6,066
Cimatella	VII	2,098	42	14	13	08	56	28	3	0.82	0.15	18.3	25.24	17.6	3.5	32,780	6,459
Punta Artica	VIII	2,327	42	15	51	08	58	18	2	1.25	0.1	8	29.88	13.6	1.5	42,270	4,589
Lavu Bellebone*	Ku98	2,338	42	12	32	09	03	28	8	0.112	0.019	17	32.87	10 (7)	2.2	3,410	630

Column 7, blank-corrected, NIST SRM 4325 ^{10}Be-standard, but 1.51 Ma half-life according to Gosse and Phillips (2001), 1σ error of the measurements (column 8), production rates (column 10) after Dunai (2000), corrected for topographic shielding (measured from panorama photos; column 6) and average temperature during exposure time. For the calculation of erosion rates (column 11) we assume that ^{10}Be production equals erosion (''steady state'') with related 1σ error (column 12). For comparison, the nominal exposure age is given (column 13), assuming zero erosion. The last sample (*) has been measured by P. Kubik, ETH Zürich (personal communication)

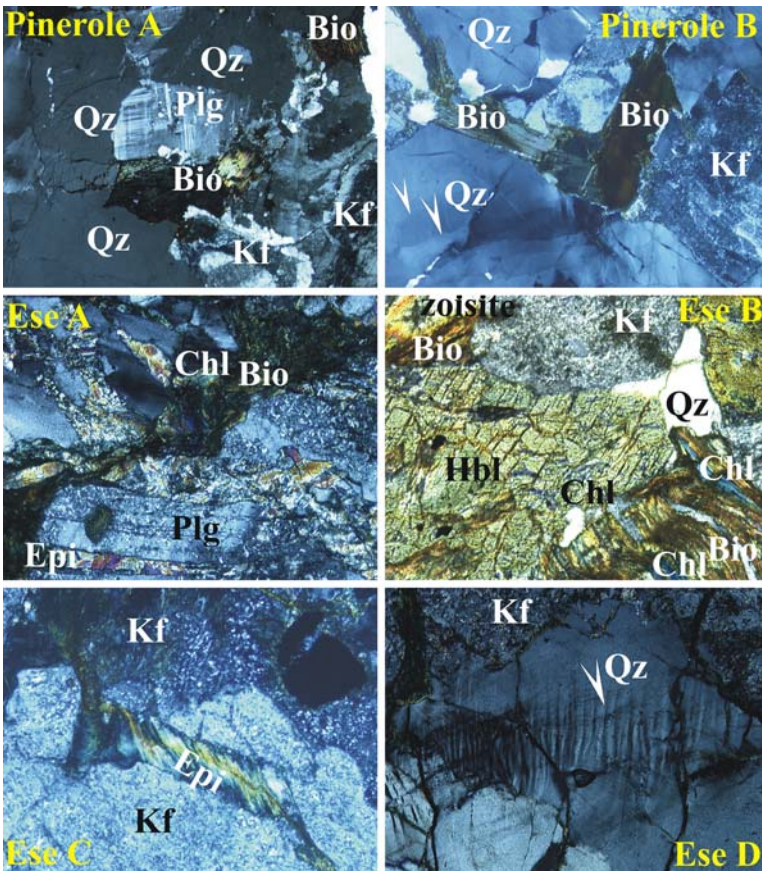

Fig. 13 Thin sections of sites I and II (*cores*) from 20 cm depth. The upper two sections form Pinerole show almost fresh biotite (*Bio*), minor alteration of plagiocase (*Plg*) and of perthite (*Kf*), and partly undulatory extinction of quartz (*white arrows*). The other sections from the Ese plateau show high alteration of biotite, amphibole (*Hbl*) and perthite, new formation of chlorite (*Chl*), zoisite and epidote (*Epi*), saussuritisation of plagioclase, and deformation lamellae (*white arrows*) with some brittle quartz deformation

Table 2 Concentration of ^{10}Be in the core samples from the surface to 30 cm depth

Sample code	Depth (cm)	Altitude (m)	N: conc. ^{10}Be × 10^6 at/g	Error
Niolu_I_15	1.50	1,759	1.23	0.11
Niolu_I_52	5.20	1,759	1.20	0.11
Niolu_I_99	9.90	1,759	1.23	0.11
Niolu_I_174	17.40	1,759	1.09	0.13
Niolu_I_285	28.50	1,759	0.87	0.10
Ese_II_15	1.50	1,759	0.55	0.11
Ese_II_100	10.00	1,759	0.39	0.13
Ese_II_272	27.20	1,759	0.30	0.12

gests that the erosion rate determined at the surface may in fact be close to the lower two sigma error limit (8.4 instead of 9.1 mm/kyear erosion). Unfortunately, the three samples of core II are insufficient to make a more precise determination of this effect.

If only the calc-alkaline granite sampling sites are considered, a tendency for westward increasing erosion rates is observed in the north (Table 3), which matches the regional precipitation trend in a fairly well documented reference level at about 900 m a.s.l., but mismatches extrapolated upward increasing precipitation rates at our sampling sites, since precipitation data from stations above 1,000 m are almost lacking (see Bruno et al. 2001, p. 24). More likely, precipitation isolines do not strictly depend on elevation, as calculated by Bruno et al. (2001), but steeply rise above the northern interior in the course of foehn effects (Fig. 15). The foehn effect of temperature rise and precipitation drop matches with the change of vegetation from maritime forest (*Fagus sylvatica*, *Abies alba*) on the western windward side and dry pine forest (*Pinus nigra* ssp. *laricio*) on the interior leeward side (Fig. 15). Moreover, the treeline rises from the western side to the interior by >300 m, indicating a rise of annual temperature by ~2°C. Weathering of bare rock probably depends not only on the amount of precipitation, but also on the presence of moisture and frequency of wetness, as indicated by vegetation. The distribution of this vegetation zone largely matches the zone of highest frequency of cloud cover (Meerkötter et al. 2004). The trend of eastward decreasing exposure of the sites to wind hampers discrimination of its quantitative role for erosion. Erosion rates obtained close to the drainage divide in the west match with those in the southwest.

The type and amount of the most weatherable mineral in the calc-alkaline granites has no obvious

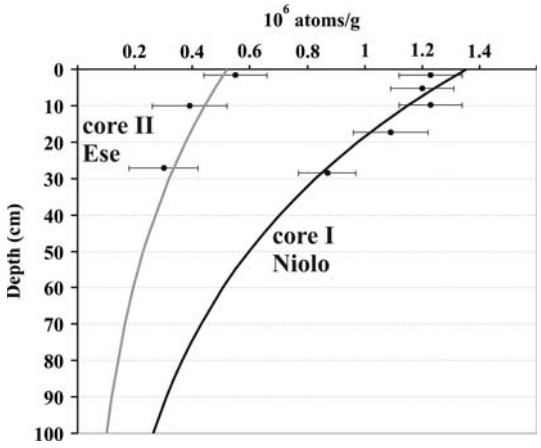

Fig. 14 Modelled vertical profile of ^{10}Be concentrations in two 30 cm-deep granite cores from 1,759 m a.s.l. in south-central and northern Corsica

effect on measured erosion rates. In the presence of water, calc-alkaline granites are affected by relatively fast hydrolysis of biotite, which expands microcracks and grain boundaries. In Corsica, initial hydrolysis of biotite in calc-alkaline granites has been detected 0.5 m below bare bedrock surface (Klaer 1956). As a result, calc-alkaline granite surfaces disintegrate into mm-sized grains to produce grusy regolith. Compared to the calc-alkaline granites, alkali-feldspar granite is apparently more resistant to weathering, since mountains built of alkali-feldspar granite rise above the surrounding calc-alkaline granite landscape. Nevertheless, the erosion rates calculated for sample V (8.2 mm/kyear) does not differ significantly from the lowest erosion rate found in calc-alkaline granite sample I (9.1 mm/kyear), especially if the depth profile is considered. It seems that the higher weathering resistance of the alkali-feldspar granite (V) is balanced by the higher precipitation.

The degree of brittle deformation of the rock plays a role for long-term erosion rates, although the effect is not very strongly reflected by our samples from the recently inactive regional setting of Corsica. The strongly foliated sample VI displays the highest erosion rate, and comparison of calc-alkaline granite deformation features qualitatively supports the trend towards increased erosion rates.

Implications

Freshly abraded granite, even calc-alkaline granite, seems to weather slower than constantly exposed rock castles, which is not surprising. The difference in erosion rates, however, is not large, even if the different precipitation rates are considered.

Our results show the importance (1) of precipitation/moisture, and (2) of the degree of brittle deformation (shearing) for erosion rates, whereas the weathering resistivity of minerals of granitic rocks on summit surface relics appears to play a limited role. The effect of differential weathering resistivity be-

Table 3 Climate and weathering properties of sampling sites

Column 1 Sampling site	2 Code	3 Altitude (m)	4 Pp (mm/a) at ~900 m	5 Exposure to wind	6 Granitoid type	7 Weatherable mineral (%)	8 Weathering sensitivity	9 Degree of brittle deformation	10 Erosion rate (mm/kyear)	11 Nom. expo. age (kyear)
Pinerole/ Niolu	I	1,759	850*	Low	Calcalkaline	Biotite 7–10	High	Low	9.1	63
Plateau d'Ese	II	1,759	1,320*	Moderate	Calcalkaline	Plagioclase ~40	Moderate	High	20.3	28
Mte Giovanni	III	1,950	1,320*	High	Calcalkaline	Biotite 5–7	High	Moderate	14.0	41
Mte Renoso	IV	2,352	1,320*	High	Calcalkaline	Biotite 5–8	High	Moderate	15.2	38
Bavella	V	1,420	>1,100	Very low	Alkaline	Hastingsite ~10	Low	Very low	8.2	70
Tenda	VI	1,453	1,000–1,100	Moderate	Orthogneiss	Plagioclase ~40	Moderate	Very high	24.2	24
Cimatella	VII	2,098	1,250*	High	Calcalkaline	Biotite 7–10	High	Moderate	17.6	33
Punta Artica	VIII	2,327	900–1,000	Moderate	Calcalkaline	Biotite 7–10	High	Low	13.6	42
Lavu Bellebone	Ku98	2,338	1,400–1,500	Very low	Calcalkaline	Biotite 7–11	High	Low	12	3

Annual precipitation in the reference level of ~900 m a.s.l. either close to a climate station (marked with asterisk*) or estimated from an interpolated precipitation map (Bruno et al. 2001; column 4). Exposure to wind refers to a qualitative estimate of local maximum wind speed, based on local topography, rock pavements and records of automatic climate stations of the French Meteorologic Service (column 5). Sensitivity to chemical weathering is indicated by the percentage of the most weatherable mineral of the samples (column 7) and qualitative differences of rock surface freshness (column 8). Mechanical weathering resistance referring to the degree of brittle deformation is qualitatively estimated (column 9). An estimate of the latest unlikely, but possible ice cover is based on Kuhlemann et al. (2005b) and yet unpublished results of the glaciation history (column 12)

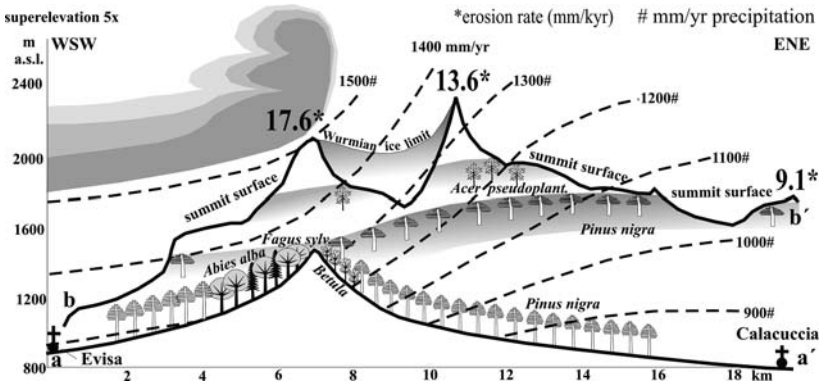

Fig. 15 WSW-ENE cross sections in northern Corsica to illustrate potential precipitation and vegetation trends (for location of profiles see Fig. 7). The lower profile a–a′ connects the climate stations Evisa (1,250 mm/year) and Calacuccia (850 mm/year, Table 2) across the Vergio pass. The upper profile b–b′ follows the crest of the sampling sites VII, VIII, and I. The precipitation isolines are hand-fitted to relief and the foehn effect indicated by vegetation. The *uppermost treeline* is represented by isolated stands of *Acer pseudoplatanus* (and *Sorbus aucuparia*). A continuous treeline is formed by *Pinus nigra* ssp. *laricio* and *Fagus sylvatica*

comes more obvious in the landscape, where fluvial erosion and glaciation carved out brittle fault zones to form deep and wide valleys, and shaped steep walls around alkali-feldspar granite intrusions. Here, erosion is limited by weathering and hillslope processes. On the summit surface, where erosion rates are limited both by weathering rate and transport, the relative erodibility differences are less strongly reflected by geomorphology. Alkaline granites, however, always rise above surrounding calc-alkaline granites. According to the geodynamic history of Variscan Corsica (Danisik 2005) these large-scale features had up to 17 Myears time to develop.

The calculated erosion rates are relatively high with respect to a preservation of inferred Early Miocene landscapes. An average erosion rate of 8–20 m/Myear in low relief sites without fluvial erosion would mean c. 130–350 m of erosion since the end of the Early Miocene, which should have largely destroyed an ancient landscape. Nevertheless, three factors support a preservation of the shape of old landscapes in southern Corsica:

1. A lowering of a Early Miocene relief by etching, which preserved the morphologic character of the ancient landscape, not the original surface.
2. A temporary shallow burial, which facilitated re-exhumation of the ancient surface: There is evidence for a temporary burial by Middle Miocene tuffs and fluvial deposits in the south of Corsica, since tuffs are preserved in the foothills (Ottaviani-Spella et al. 2001) within an etched paleosurface. (U-Th/He) ages indicate that paleosurfaces at different elevation were in fact part of the same continuous surface (Danisik 2005).
3. A Pleistocene increase of erosion rates exceeding those of the Middle and Late Miocene: apatite fission track data (Danisik 2005) indicate accelerated erosion in the last millions of years, probably due to high climate variability (Zhang et al. 2001).

Erosion rates from high-elevation sites can be compared with post-glacial bedrock incision in low-gradient, U-shaped valleys at elevations which were occupied by glaciers until the end of the last glacial maximum (LGM) and which have not been abraded by ice during the late glacial (Kuhlemann et al. 2005b). Fluvial bedrock channel incision ranges between 5 and 8 m in longitudinal sections with relatively strong local gradients (Table 4), in catchments of 5–30 km^2 size. This is equivalent to about 250–450 mm/kyear maximum incision rate. Representative average incision rates are difficult to assess since longitudinal slopes in glacial valleys of Corsica strongly vary, but half of these values may be a guess. Edges of the narrow bedrock channels in glacial valleys are always angular and irregular, excluding glacial overprint after fluvial incision. A similar range of postglacial incision in terraces is also observed in larger mountain catchments between 900 and 70 m a.s.l., well below the extent of glaciers (Table 4). Pleistocene moraines of up to 20 m thickness were incised prior to bedrock incision. The formation of some of these terraces has been attributed to the LGM (Conchon 1975, 1989), but fluvial incision prior to the LGM cannot be excluded.

The late Pleistocene and Holocene bedrock incision rates are about an order of magnitude higher than erosion rates on summit surface relics, resulting in an increase of relief. A similar relative difference, at lower absolute erosion rates and incision rates, is found in

Table 4 Fluvial incision in bedrock and glacial terraces in glacial valleys (upper part) and valleys below the glaciation limit (lower part)

Column 1	2	3	4			5			6	7
River	Location	Altitude (m)	N. latitude			E. longitude			Incision since ka	Incision bedrock (m)
			°	′	″	°	′	″		
Spasimata	Ref. Carrozzu	1,215	42	25	27	08	53	56	18	8
Tighiettu	Haut Ascu	1,488	42	23	24	08	55	30	15	5
Colga/Niolu	Forest Serv. Poppaghia	1,370	42	16	02	08	55	51	18	5
Tavignano	Berg. de Tramizzole	1,410	42	14	48	08	59	52	18	8
Zoicu	Berg. de Izzola	1,270	42	12	46	08	57	08	18	6
Manganello	Berg. de Tolla	950	42	10	04	09	06	03	18	8
Agnone	Vizzavona, Berg. ruins	1,490	42	07	04	09	05	28	18	6
Prunelli	Berg. de Arbajola	1,560	42	02	07	09	07	00	18	6
Polischellu	Bavella	600	41	49	21	09	15	21	18	8
Figarella	Forest Serv. Bonifatu	500	42	26	31	08	51	26	18?	8
Golo	Francardo	250	42	24	14	09	11	55	18?	8
Fango	Tuvarelli	90	42	23	00	08	45	05	18?	7
Porto	Spelunca	215	42	15	17	08	45	58	18?	7
Fium Orbu	Ghisoni	380	42	06	10	09	14	59	18?	6
Gravona	Bocognano	552	42	05	30	09	04	06	18?	4
Prunelli	Bastelica	877	42	00	14	09	04	25	18?	3
Solenzara	Camping Rosumarinu	70	41	50	40	09	20	37	18?	9

Incision is measured on photos and with an electronic altimeter (1 m resolution on display, precision of measurement ~0.25 m). Error is ±1 m

? represents the age uncertainty

western America (Small et al. 1997). Here, limited isostatic response to mass removal from the valleys, due to flexural rigidity of the continental lithosphere, largely suppresses surface uplift of the summits. In contrast, Corsica is surrounded by oceanic and strongly thinned continental lithosphere. Eroded material is largely evacuated from the island and exported to surrounding deep basins. Thus, mass evacuation from the valleys is largely compensated by isostatic uplift. As a result, relief increases and peaks are uplifted as the valleys are deepened and widened at the expense of the paleosurface relics.

Discussion

Two crucial assumptions have been made in this paper. The first one is dynamic equilibrium of erosion rates and nuclide production rates, which may be called ''steady state''. The second is the rejection of a relevant role of ice at the sampling sites during stadials, either for shielding or for removal of rocky material to create fresh exposures.

The first assumption is based on the fact that chemical dissolution or grusification of granitoids means that the erosion processes in the sampling sites are characterized by many small increments. Spallation of larger rock fragments as a dominant physical weathering process works in the opposite mode, which means large increments but rare events. In the latter case several samples of one single tor are required to constrain the timing of several spallation events (see Small et al. 1997). With grusy weathering or dissolving sites, multiple sampling is not required.

The second assumption is more complex for most sites. Two sites (I, V) remained below the local snowline for the entire Wurmian (Kuhlemann et al. 2005b). The other sites were located above the snowline for part or much of the Wurmian (III, IV, VII, VIII), including the late Wurmian. However, field observation suggests that during the Wurmian rock castles were not destroyed by glacial erosion. Spallation most likely was more frequent during glacial times, but as long as the size of spalled rock chips remained below 150 mm, at average erosion rates exceeding 10 mm/kyear, equilibrium would have been achieved after the LGM (see Small et al. 1997). A more serious problem is a possible cover by non-erosive ice. It is documented from eastern Canada (Marquette et al. 2004) and Sweden (Fabel et al. 2002) that cold-based non-erosive ice had covered and preserved ancient landscapes with tors and regolith cover. Nevertheless, the sampling sites in Corsica could only have been covered by wet-based temperate ice, due to the oceanic climate at higher altitudes. It is unlikely that boulders of rock castles placed on the margin of a summit surface relict

were not pulled over the edge if this surface was capped by ice thick enough to shield the tens of meters high tors from cosmic rays. Accumulation of ice on the summit surface relics was probably limited by strong winds along the main drainage divide. Site VII on a mountaintop probably also remained free of any significant ice cover.

The compilation of Cockburn and Summerfield (2004) notes quite similar erosion rates in seasonally wet temperate to alpine settings of western America and southeastern Australia. The lowest erosion rates are found by Small et al. (1997) in the Sierra Nevada, but this paper does not mention differences in climate, degree of deformation or petrography in the four studied western American summit surfaces (3,300–3,750 m a.s.l.). It seems that in this fairly continental alpine climate setting, frost weathering as the dominant process is less effective than grusification and dissolution in probably wetter, temperate to subalpine climate in Corsica. This hypothesis, however, cannot be substantiated without detailed information on the western America sites.

The impact of precipitation, degree of deformation, and petrography on erosion rates, as reflected in our data, is apparently in conflict with conclusions drawn from studies of ^{10}Be concentrations in small catchments of various climatic setting (Riebe et al. 2000; Von Blanckenburg et al. 2004). These studies, however, show a fairly wide scatter of data particularly in mid latitudes. These data clearly show that ongoing tectonic activity strongly increases erosion rates, possibly by an order of magnitude. Thus, second-order factors such as climate, degree of deformation, and petrography can only be detected if study areas that have experienced recent tectonic deformation are not being compared with tectonically inactive (including passively uplifting) areas.

Conclusions

Erosion rates on the summit surfaces in Corsica range between 8 and 24 mm/kyear, similar to other granitic study areas of temperate to subalpine climate. The erosion rates in Corsica depend mainly on the degree of brittle deformation, local precipitation, and petrographic composition of granites. It remains unclear if this dependency is a general rule, since former studies do not provide enough details of these factors.

Chemical erosion dominates subalpine climate conditions in Corsica at elevations between 1,700 and 2,300 m. Dissolution or disintegration to mm-sized grains (grusification) justify an interpretation of cosmogenic nuclide concentrations in terms of average erosion rates. The erosion rates that were obtained apparently contradict a preservation of Early Miocene landscapes. However, temporal burial in the Middle Miocene and lower erosion rates prior to ~3 Ma probably supported their preservation. Their destruction is accelerated through the glacial widening and deepening of valleys, and plucking at the plateau margins. Valley incision rates an order of magnitude higher than erosion rates on summit surfaces result in relief enhancement and surface uplift.

Acknowledgments This study has been funded by the German Science Foundation (DFG Project Ku 1298/2). We are obliged to Martin Staiger for technical support in core drilling on top of tors and Gerlinde Kost, Dagmar Höckh and Dorothea Mühlbayer-Renner for purification of quartz samples. We thank Greg Balco (Seattle) for technical advice for quartz purification, and Peter Kubik (Zürich) for measuring the exposure age of a Holocene roche moutonnée. The samples were processed by Ingrid Krumrei in the frame of DFG Project Ku 1298/7. Constructive reviews by Peter Molnar, Robert Anderson, and anonymous reviewers helped to improve an earlier version of this paper. The present manuscript benefitted from reviews of Derek Fabel, Kevin Norton and Friedhelm v. Blanckenburg.

References

Anderson RS (2002) Modeling of tor-dotted crests, bedrock edges and parabolic profiles of the high alpine surfaces of the Wind River Range, Wyoming. Geomorphology 46:35–58

Bierman P, Turner J (1995) ^{10}Be and ^{26}Al evidence for exceptionally low rates of Australian bedrock incision and the likely existance of pre-Pleistocene landscapes. Quat Res 44:378–382

Brook EJ, Brown ET, Kurz MD, Ackert RP Jr, Raisbeck GM, Yiou F (1995) Constraints on age, erosion, and uplift of neogene glacial deposits in the Transantartic Mountains determined from in situ cosmogenic ^{10}Be and ^{26}Al. Geology 23:1063–1066

Brunet C, Monie P, Jolivet L, Cadet JP (2000) Migration of compression and extension in the Tyrrhenian Sea, insights from ^{40}Ar/^{39}Ar ages on micas along a transect from Corsica to Tuscany. Tectonophysics 321:127–155

Bruno C, Dupré G, Giorgetti G, Giorgetti JP, Alesandri J (2001) Chì tempu face? Météorologie, climat et microclimates de la Corse: CNDP-CRDP de Corse/Météo France. Ajaccio, France, pp 138

Cacho I, Grimalt JO, Canals M (2002) Response of the Western Mediterranean Sea to rapid climatic variability during the last 50,000 years, a molecular biomarker approach. J Mar Sys 33–34:253–272

Cavazza W, Zattin M, Ventura B, Zuffa GG (2001) Apatite fission-track analysis of Neogene exhumation in northern Corsica (France). Terra Nova 13:51–57

Cockburn HAP, Summerfield MA (2004) Geomorphological applications of cosmogenic isotope analysis. Prog Phys Geogr 28:1–42

Cockburn HAP, Brown RW, Summerfield MA, Seidl MA (2000) Quantifying passive margin denudation and landscape development using a combined fission-track thermochro-

nology and cosmogenic isotope analysis approach. Earth Planet Sci Lett 179:429–435
Conchon O (1975) Les formations quaternaires de type continental en Corse orientale. PhD Thesis, University of Paris VI, vol I: Observations et interprétations, 514 pp, vol II: Documents annexés, 244 pp
Conchon O (1985) Nouvelles observations sur les formations glaciaires quaternaires en Corse. Bull Assoc Fr Quat 1:5–11
Conchon O (1986) Quaternary glaciations in Corsica. In: Sibrava V, Bowen DQ, Richmond GM (eds) Quaternary glaciations in the Northern Hemisphere. Quat Sci Rev 5:429–432
Conchon O (1989) Dynamique et chronologie du détrisme quaternaire en Corse, domaine Méditer-ranéen montagnard et littoral. Bull Assoc Fr Etud Quat 4:201–211
Clark DH, Bierman PR, Larsen P (1995) Improving in situ cosmogenic chronometers. Quat Res 44:367–377
Danisik M (2005) Cooling history and relief evolution of Corsica (france) as constrained by fission track and (U-Th)/He thermochronology. Tübinger Geowiss Arb A 72:130
Dunai TJ (2000) Scaling factors for production rates of in-situ produced cosmogenic nuclides: a critical reevaluation. Earth Planet Sci Lett 176:157–169
Dunai TJ (2001a) Reply to comment on ''scaling factors for production rates of in situ produced cosmogenic nuclides: a critical reevaluation'' by Darin Desilets, Marek Zreda and Nathaniel Lifton. Earth Planet Sci Lett 188:289–298
Dunai TJ (2001b) Influence of secular variation of the geomagnetic field on production rates of in situ produced cosmogenic nuclides. Earth Planet Sci Lett 193:197–212
Fabel D, Stroeven AP, Harbor J, Kleman J, Elmore D, Fink (2002) Landscape preservation under Fennoscandian ice sheets determined from in situ produced ^{10}Be and ^{26}Al. Earth Planet Sci Lett 201:397–406
Ferrandini M, Ferrandini J, Loye-Pilot MD, Butterlin J, Cravatte J, Janin MC (1998) Le Miocène du bassin de Saint-Florent (Corse); modalités de la transgression du Burdigalien supérieur et mise en evidence du Serravallien. Geobios 31:125–137
Ferrandini L, Rossi P, Ferrandini M, Farjanel G, Ginsburg L, Schuler M, Geissert F (1999) La Formation conglomératique du Vazzio près d'Ajaccio (Corse-du-Sud), un témoin des dépôts du Chattien supérieur continental synrift en méditerranée occidentale. C R Acad Sci (Paris) Sér II Sci Terre et Planèt 329:271–278
Gorini C, Le Marrec A, Mauffret A (1993) Contribution to the structural and sedimentary history of the Gulf of Lions, (Western Mediterranean), from ECORS profiles, industrial seismic profiles and well data. Bull Soc Géol France 164:353–363
Gosse JC, Phillips FM (2001) Terrestrial in situ cosmogenic nuclides: theory and application. Quat Sci Rev 20:1475–1560
Hayes A, Kucera M, Kallel N, Sbaffi L, Rohling EJ (2005) Glacial Mediterranean sea surface temperatures based on planktonic foraminiferal assemblages. Quat Sci Rev 24:999–1016
Hormes A, Müller BU, Schlüchter C (2001) The Alps with little ice: evidence für eight Holocene phases of reduced glacier extent in the Central Swiss Alps. Holocene 11:255–265
Ketcham RA, Donelick RA, Donelick MB (2000) AFTSolve: a program for multi-kinetic modelling of apatite fission-track data. Min Soc Am Geol Mater Res 2:1–32
Klaer W (1956) Verwitterungsformen im Granit auf Korsika: Petermanns Geogr Mitt Erg 261:1–146
Kohl CP, Nishiizumi K (1992) Chemical isolation of quartz for measurement of in-situ-produced cosmogenic nuclides. Geochim Cosmochim Acta 56:3583–3587
Kubik PW, Ivy-Ochs S (2004) A re-evaluation of the 0–10 ka 10Be production rate for exposure dating obtained from the Köfels (Austria) landslide. Nucl Instrum Methods Phys Res B 223–224:618–622
Kubik PW, Ivy-Ochs S, Masarik J, Frank M, Schlüchter C (1998) ^{10}Be and ^{26}Al production rates deduced from an instantaneous event within the dendro-calibration curce, the landslide of Köfels, Ötz valley, Austria. Earth Planet Sci Lett 161:231–241
Kuhlemann J, Székely B, Dunkl I, Molnár G, Timár G, Frisch W (2005a) DEM analysis of mountainous relief in a crystalline basement block, Cenozoic relief generations in Corsica (France). Z für Geomorph N F 49:1–21
Kuhlemann J, Frisch W, Székely B, Dunkl I, Danišik M, Siegers I (2005b) Würmian maximum glaciation in Corsica. Aust J Earth Sci 97:68–81
Lal D (1991) Cosmic ray labeling of erosion surfaces, in situ nuclide production rates and erosion models. Earth Planet Sci Lett 104:424–439
Lenôtre N, Ferrandini J, Delfau M, Panighi J (1996) Mouvements verticaux actuels de la Corse (France) par comparaison de nivellements.- Comptes Rendus de l'Academie des Sciences, Serie II. Sci Terre Planet 323:957–964
Marquette GC, Gray JT, Gosse JC, Courchesne F, Stockli L, Macpherson G, Finkel R (2004) Felsenmeer persistence under non-erosive ice in the Torngat and Kaumajet mountains, Quebec and Labrador, as determined by soil weathering and cosmogenic nuclide exposure dating. Can J Earth Sci 41:19–38
Masarik J, Reedy RC (1996) Monte Carlo simulation of in situ-produced cosmogenic nuclides. Radiocarbon 38:163–164
Meerkötter R, König C, Bissolli P, Gesell G, Mannstein H (2004) A 14-year European cloud climatology from NOAA/AVHRR data in comparison to surface observations. Geophys Res Lett 31:L15103. doi:10.1029/2004GL020098
Nishiizumi K, Winterer EL, Kohl CP, Klein J, Middleton R, Lal D, Arnold JR (1989) Cosmic ray production rates of ^{10}Be and ^{26}Al in quartz from glacially polished rocks. J Geophys Res 94:17907–17915
O'Brien SR, Mayewski PA, Meeker LD, Meese DA, Twickler MS, Whitlow SI (1995) Complexity of Holocene climate as reconstructed from a Greenland ice core. Science 270:1962–1964
Orszag-Sperber F, Pilot MD (1976) Grands traits du Néogène de Corse. Bull Soc Géol Fr 18:1183–1187
Ottaviani-Spella M, Girard M, Rochette P, Cheilletz A, Thinon M (2001) Le volcanisme acide burdigalian du Sud de la Corse: pétrologie, datation K-Ar, paléomagnétisme. C R Acad Sci (Paris) Sci Terre Planèt 333:113–120
Riebe CS, Kirchner JW, Granger DE, Finkel RC (2000) Erosional equilibrium and disequilibrium in the Sierra Nevada, inferred from cosmogenic ^{26}Al and ^{10}Be in alluvial sediment. Geology 28:803–806
Rossi P, Cocherie A (1991) Genesis of a Variscan batholith; field, petrological and mineralogical evidence from the Corsica-Sardinia Batholith. Tectonophys 195:319–346
Rossi P, Rouire J, Durand-Delga M (1980) Carte geólogique de la Corse A 1/250 000, Notice explicative de la feuille. Bureau Rech Géol Miniéres, Service Géol National, Orleans
Schaller M, Von Blanckenburg F, Veldkamp A, Tebbens LA, Horvius N, Kubik PW (2002) A 30 000 yr record of erosion rates from cosmogenic ^{10}Be in Middle European river terraces. Earth Planet Sci Lett 204:307–320
Seager WR, Mack GH, Lawton TF (1997) Structural kinematics and depositional history of a Laramide uplift-basin pair in

southern New Mexico; implications for development of intraforeland basins. GSA Bull 109:1389–1401

Seidl G (1978) Geologie und geodynamische Entwicklung der Schistes Lustres-Zone und des Randbereichs des westkorsischen Altkristallins zwischen Asco und der Plaine Orientale (NE-Korsika). Unpubl Diss Univ Munich, Germany, pp 1–112

Small EE, Anderson RS (1998) Pleistocene relief production in Laramide mountain ranges, western United States. Geology 26:123–126

Small EE, Anderson RS, Repka JL Finkel R (1997) Erosion rates of alpine bedrock summit surfaces deduced from in situ ^{10}Be and ^{26}Al. Earth Planet Sci Lett 150:413–425

Stone JO (2000) Air pressure and cosmogenic isotope production. J Geophys Res 105(B10):23753–23759

Vigliotti L, Langenheim VE (1995) When did Sardinia stop rotating? New paleomagnetic results. Terra Nova 7:424–435

Von Blanckenburg F, Hewawasam T, Kubik P (2004) Cosmogenic nuclide evidence for low weathering and denudation in the wet tropical Highlands of Sri Lanka. J Geophys Res 109:F03008. doi:10.1029/2003JF000049

Zarki-Jakni B, Van der Beek P, Poupeau G, Sosson M, Labrin E, Rossi P, Ferrandini J (2004) Cenozoic denudation of Corsica in responce to Ligurian and Tyrrhenian extension, results from apatite fission-track thermochronology. Tectonics 23. doi:10.1029/2003TC001535

Zhang P, Molnar P, Downs WR (2001) Increased sedimentation rates and grain sizes 2–4 Myr ago due to the influence of climate change on erosion rates. Nature 410:891–897